4. RESULTS AND DISCUSSION

My thesis aims to define the role of OsFT-L1 during the floral transition and in determining inflorescence architecture, focusing on its molecular characterization during the reproductive development of rice.

To tackle this topic, I carried out a series of experiments through genetic, molecular and imaging approaches discussed below.

4.1 A REGULATORY MODULE INVOLVING THREE FLORIGENS AT THE SAM

Thanks to an RNA-seq performed in my lab in 2019, comparing the transcripts from SAM of plants exposed to SD conditions and plants that remained in LD conditions, we obtained a list of genes differentially expressed during floral commitment[50].

Among the genes that were induced at the SAM, together with *OsMADS14*, *OsMADS15* and *OsMADS34,* we identified *FLOWERING LOCUS T-LIKE 1 (FT-L1).* This gene, a member of the phosphatidyl-ethanolamine-binding proteins (PEBP), encodes a florigenic protein closely related to Hd3a, RFT1 and AtFT with which it shares a high homology in the aminoacidic sequence[49] (fig.25).

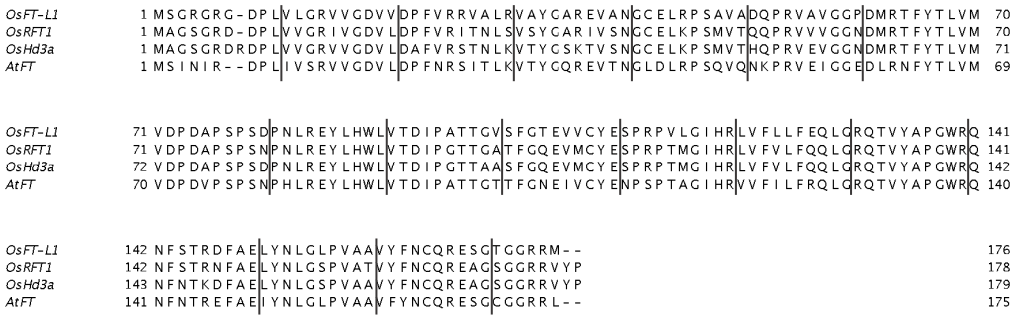

Figure 25 - Alignment of FT-L1 with RFT1, Hd3a and Arabidopsis thaliana FT. *Sequences for rice proteins (OsFT-L1, OsRFT1 and OsHd3a) were taken from MSU (rice) and for Arabidopsis from TAIR (AtFT). Note that LOC_Os01g11940.1 is misannotated with the first 100 amino acids having no homology with the other florigens. Alignments from the second Methionine give perfect protein match.*

Plants overexpressing FT-L1 under the control of a constitutive promoter flower during regeneration in tissue culture with stamen-like and pistil-like organs in ectopic positions, indicating that FT-L1 has strong flower-inducing functions[18].

These data suggest that *FT-L1* could have an important role in rice flowering and that its function may be downstream of *Hd3a* and *RFT1.*

4.1.1 *FT-L1* expression directly depends from florigens and photoperiod

To investigate the transcriptional dependency of FT-L1 upon the two florigens, we have performed a qRT-PCR to quantity the transcripts of this gene in leaf and meristem tissues, both in Nipponbare wt lines and in the Nipponbare *hd3a rft1* double knock-out mutant, whose plants are unable to flower (fig.26A). (*Mineri et al., manuscript submitted, see Appendix 4 for the entire manuscript)*

For what concerns the expression in meristem tissue, in the WT it was observed an increase in gene expression together with the progression of panicle development, reaching a peak and then a plateau at the floret meristem stage. In the double mutant, *FT-L1* transcripts are not detectable revealing that the presence of functional *Hd3a* and *RFT1* is essential for *FT-L1* induction (fig.26B).

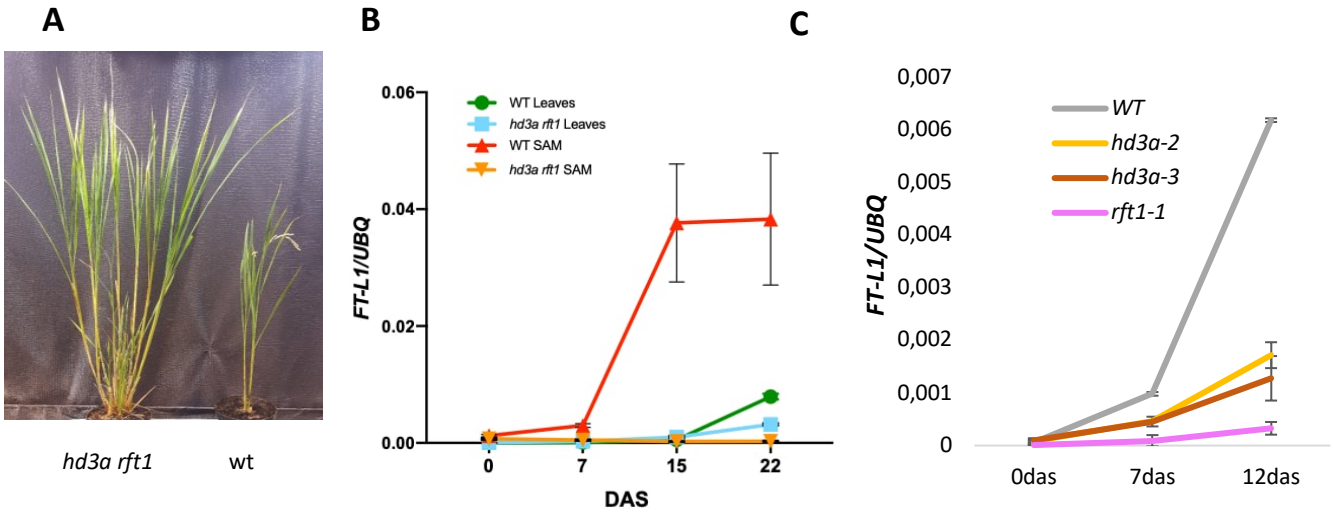

Figure 26 – Spatio-temporal regulation of FT-L1 expression. *A. Picture of an hd3a rft1 double mutant unable to flower even after 3 years of growth under SD. B. Temporal expression of FT-L1, in SAMs and leaves of wild type and hd3a rft1 mutants. Samples were collected after shifting two-month-old plants from LD to inductive SD conditions C. Quantification of FT-L1 expression in apices of Nipponbare WT and Nipponbare single mutants hd3a and rft1 at different time points after the shift LD-> SD. Each time point in B and C is represented as mean ± standard deviation of two biological and three technical replicates. Values were normalized on the housekeeper UBQ. DAS, days after shift. 0 das represents a vegetative meristem (VM) stage, 7 das corresponds to the inflorescence (IM) stage, 12-15 das corresponds to the primary branch meristem (PBM) stage, while 22 corresponds to the secondary branch meristem (SBM) stage.*

We also checked the expression of FT-L1 in meristem tissues of single mutants *hd3a* and *rft1* independent lines. In these mutants, too, the transcript abundance is very reduced in particular in *rft1*, suggesting a stronger dependency upon this florigen (fig.26C).

Conversely, in the leaves of *hd3a rft1* double mutants and in the wild type, a mild induction of *FT-L1* transcription was observed.

Since we demonstrated that FT-L1 activation depends on the florigen and on the photoperiod, we wanted to separate the effects of day length induction from those of *Hd3a* and *RFT1* on *FT-L1* transcription. We have, therefore, performed a quantification of *FT-L1* transcripts in plants grown under non-inductive LD conditions and harboring an inducible system for Hd3a or RFT1 (fig.27).

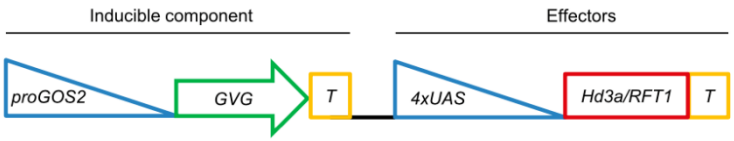

Figure 27 - Schematics of the inducible system. *The GVG chimeric protein is expressed under the GOS2 promoter to produce the inducible part of the vector. T indicates the terminator[67]. **G-V-G** is composed by **G**AL4 yeast transcription factor DNA-binding domain, **V**P16 herpes viral protein transactivating domain, and **G**R rat glucocorticoid receptor domain[93]. In the second module there are Hd3a or RFT1 coding sequences under the control of the 4x UPSTREAM ACTIVATION SEQUENCE (UAS)[67].*

These lines are composed by two modules: a GOS2 constitutive promotor driving expression of the GVG chimeric protein (**G-V-G**, composed by **G**AL4 yeast transcription factor DNA-binding domain, **V**P16 herpes viral protein transactivating domain, and **G**R rat glucocorticoid receptor domain[93]) to produce the inducible part of the vector and *Hd3a* or *RFT1* coding sequences under the control of the 4x UPSTREAM ACTIVATION SEQUENCE (UAS) to produce the effector component of the vector[67]. The lines obtained, *proGOS2:GVG 4×UAS:Hd3a* and *proGOS2:GVG 4×UAS:RFT1* were referred to as *Hd3a^{ind} and RFT1^{ind}*, respectively.

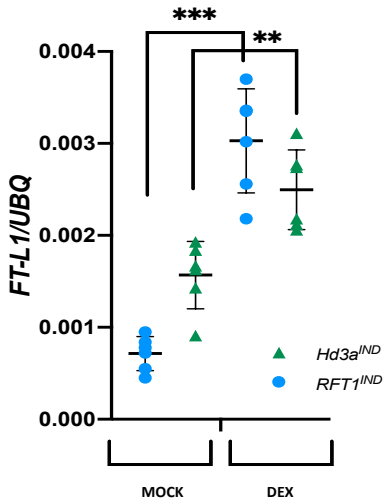

Figure 28 - Quantification of FT-L1 expression in meristems of Hd3a and RFT1 inducible plants. *Plants were grown under LD and treated with dexamethasone (dex) or mock to induce expression of either Hd3a or RFT1. SAMs were collected 16 h after the treatment. Each condition is represented by six points corresponding to two biological replicates each including three technical replicates. Values were normalized on the housekeeper UBQ. Differences are statistically different with P<0.01** and P<0.001*** based on unpaired two-tailed Student's t-test with Welch correction between dex and mock.*

FT-L1 expression increases in the apex of both inducible lines after the dexamethasone induction (fig.28).

In conclusion, we can assume the two florigens are not only necessary but also sufficient to allow *FT-L1* expression to be activated in the SAM.

To evaluate the dependency of *FT-L1* transcription from the photoperiod we run diurnal time courses to quantify *FT-L1* expression under continuous LD (fig.29A) and SD (fig.29B). These data indicate that *FT-L1* expression is not detected in LD and it is limited to SD conditions with the peak reached during the night.

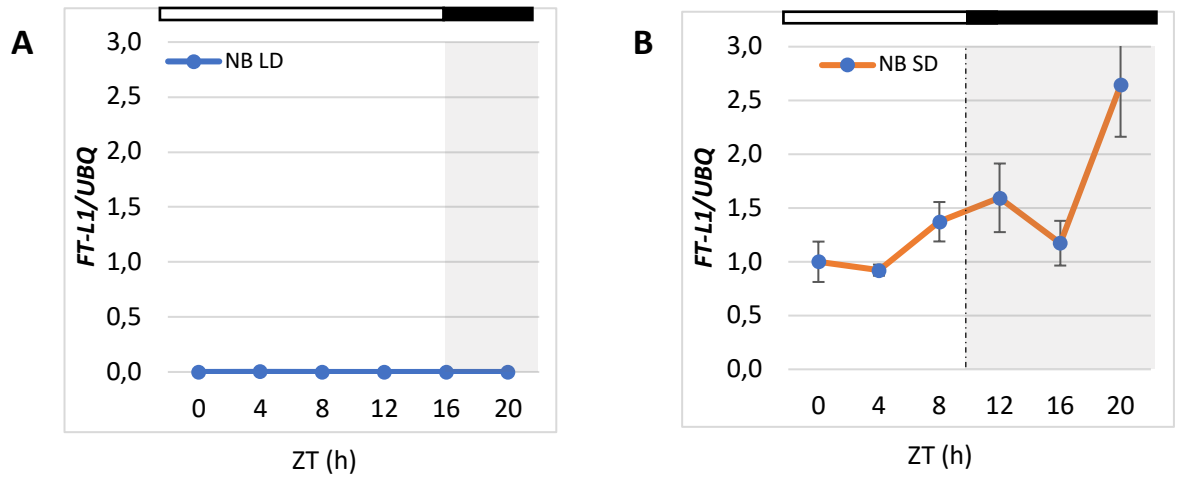

Figure 29 - Diurnal expression pattern of FT-L1 in meristems sampled under LD (A) and SD (B) photoperiodic conditions. *Nipponbare (NB) WT meristem were sampled at different time points. ZT, Zeitgeber, represents time from light on. Data are mean ± standard deviation of two biological replicates, each of which composed of three technical replicates. Values were normalized on the housekeeper UBQ.*

Taken into consideration all these evidences, data underly atypical characteristics for this gene that, despite being closely related to the florigens, shows meristematic expression. However, a specific function in the leaves could not be ruled out, in particular because *FT-L1* expression increased in leaves after the commitment, in SD conditions (fig.26B).

In order to further investigate the residue of FT-L1 expression in the leaf we quantified *FT-L1* expression in lines lacking the florigens' repressors, that strongly induce Hd3a and RFT1 transcription in leaves (fig.30). These lines, already published by Goretti et al. in 2017 include crosses between Nipponbare (NB) harboring WT alleles for the flowering repressor genes *Hd1, PRR37* and *Ghd7* and Erythroceros Hokkaido (EH) harboring mutations in these same repressors[20].

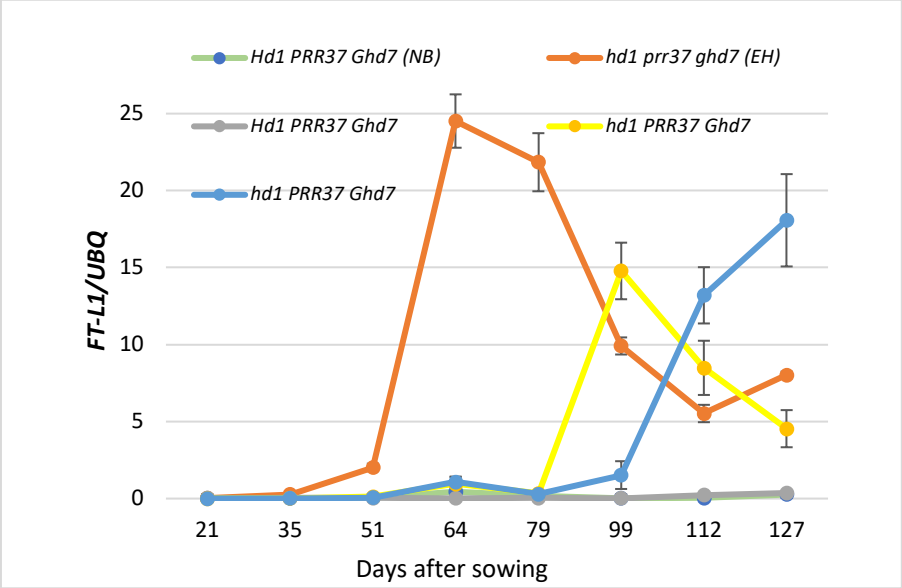

Figure 30 - Quantification of FT-L1 expression in leaves of genotypes derived from the cross between Nipponbare (NB, Hd1 PRR37 Ghd7) and Erythroceros Hokkaido (EH, hd1 prr37 ghd7). *These genotypes are described in detail in [20]. Briefly, lines inheriting mutations in Hd1, PRR37, Ghd7 or their combinations flower early and derepress Hd3a and RFT1 expression under LD. Each time is represented as mean ± standard deviation of three technical replicates and two biological ones. Values were normalized on the housekeeper UBQ.*

In the EH *hd1 prr37 ghd7* wild type background, the levels of *FT-L1* expression were very high early during a LD time course, indicating that these three flowering repressors were necessary to maintain low *FT-L1* transcription in the leaves. Two independent recombinant lines harboring only *hd1* loss-of-function alleles, also showed higher *FT-L1* expression compared to lines with functional *Hd1, PRR37* and *Ghd7* alleles.

This behavior correlates with a phenotype of early flowering of genotypes lacking *Hd1, PRR37* and *Ghd7* or *Hd1* only. Therefore, *FT-L1* is regulated by repressors of the florigens in leaves, and an increase of its transcription correlates with early flowering.

4.1.2 *FT-L1* carries out its function in the meristem

To understand whether *FT-L1* expression in leaf still holds any biological significance, indicative of a specific function in that tissue, we have performed a flowering time under LD on mis-expressing lines (fig.31).

We have cloned *FT-L1* downstream of two different tissue-specific promoters: *pOSH1*[94], that is a meristem- and stem-specific promoter and *pRPP16* [95], a vasculature-specific promoter, driving expression in companion cells and phloem parenchyma cells. We then transformed the constructs in the *FT-L1* mutant P95S (<u>*see Results and Discussion, section 4.2*</u>).

As controls, we transformed rice with an empty vector, and with *Hd3a* as main positive control.

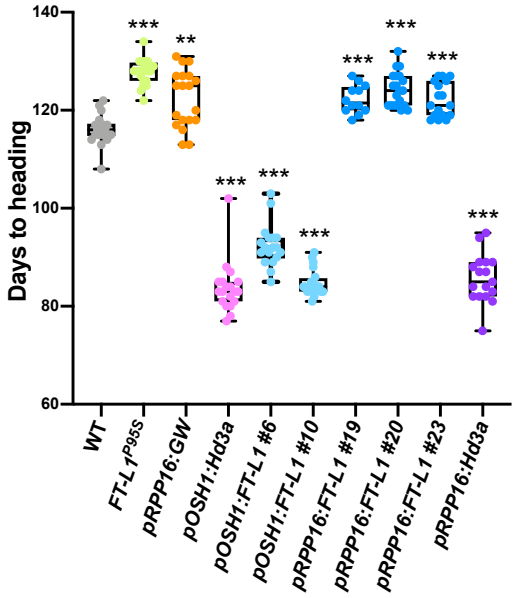

Figure 31 - Flowering time of Volano misexpressors of FT-L1 and Hd3a under LD conditions. *The background of each misexpressor line is FT-L1^{P95S}. pRPP16 is a vasculature-specific promoter while pOSH1 is meristem- and stem-specific promoter. Data are presented using box plots. ** P<0.01 and *** P<0.001 are obtained based on unpaired two-tailed Student's t-test with Welch correction between misexpressors and FT-L1^{P95S} or between FT-L1^{P95S} and the wild type. Each dot represents one plant and is color-coded depending on the genotype.*

The overexpression of *FT-L1* under *pOSH1* causes, in both independent lines, a strong early flowering phenotype, when compared to the controls WT, *FT-L1*^{P95S} and the empty vector. The same early phenotype is observed also in *pOSH1:Hd3a* and *pRPP16:Hd3a* lines. In *pRPP16:FT-L1* line, instead, no early flowering phenotype is recorded, pointing out *FT-L1* inability to rescue the mutant phenotype when mis-expressed in the leaves.

Thanks to this last approach it was possible to understand that *FT-L1* is a promoter of the floral transition acting only at the meristem and not in leaves.

4.1.3 Spatial and temporal expression of *FT-L1*

In order to obtain information about the spatial expression of *FT-L1* at the meristem, we have performed *in situ* hybridizations on Nipponbare WT tissues exposed to SD induction. As negative control, we decided to use meristems at the vegetative stage, as qPCR data indicated lack of *FT-L1* expression at this developmental phase.

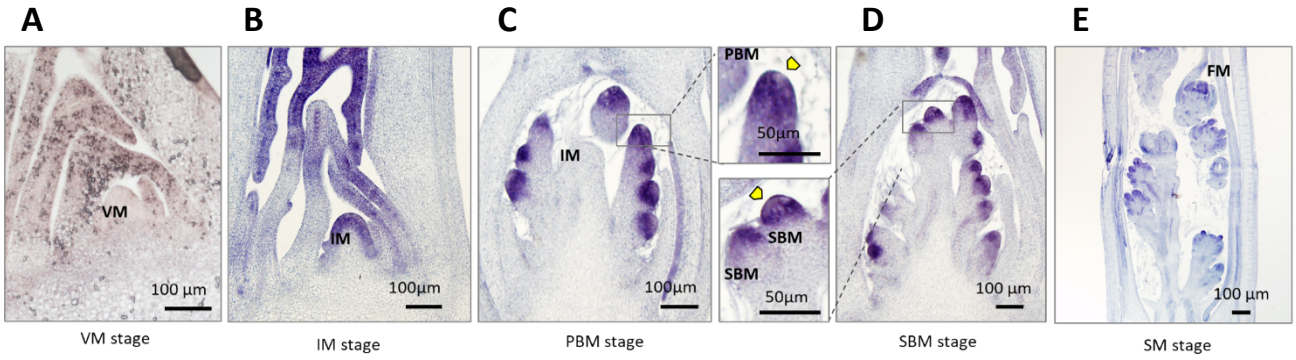

Figure 32 - In situ hybridizations of FT-L1 on wild type meristems at different developmental stages. *Longitudinal sections, 7 µm thick of Nipponbare WT meristems. A. Vegetative meristem (VM) stage, B. Inflorescence meristem (IM) stage, C. and D. Primary branch and secondary branch meristem (PBM and SBM) stages. A close-up view of PBMs and SBMs is shown to highlight expression gradients. Yellow arrowheads indicate the reduced signal at the tip of the branches at both stages. E. Floral meristem stage (FM) with floral organs already formed. For this experiment only the antisense probe was used. Experiments shown were repeated five times and with two distinct probes that gave the same results (see Material and Methods section).*

The panel of fig.32A-E shows a combination of pictures obtained together with our collaborator Taiyo Toriba, after different hybridization experiments and using two independent probes designed on *FT-L1* (*see Materials and Methods for further details*). Since hybridization signals from both probes displayed the same pattern and were consistent with each other, we are showing pictures taken from both experiments. These indicate that *FT-L1* is not expressed during vegetative growth at the SAM (fig.32A), consistent with real time data, while from inflorescence to reproductive meristems stages the expression is visible and strong. The expression at the IM is localized in the outer layers of the meristem and also in the young leaf primordia (fig.32B).

For what concerns the expression into subsequent stages, we observed a strong signal in both primary and secondary branch meristems - PBM and SBM - (fig.32C,D) suggesting a hypothetical role in these tissues. In these stages, transcription is not uniform but rather shows a gradient, with a high expression detected at the base of the branch meristem and progressively decreasing towards the tip (see yellow arrow tip). The signal, then, still persists into spikelet meristems and in the floret meristem, particularly where palea and lemma form fig.32E.

To further confirm these expression data, a *pFT-L1:eYFP* reporter line was constructed, where the expression of the reporter gene is regulated by the *pFT-L1* promoter (fig.33A-D).

The T1 generation plants were screened by PCR to select those carrying the transgene. Positive plants were grown with WT as negative control and then analyzed at the confocal. A negative control is also provided by transgenic plants at the vegetative stage.

In these transcriptional marker lines, coherently with ISH, no expression was detected in the vegetative stage (fig.33A) while the signal was observed in both primary and secondary branch stages. At these developmental phases eYFP was observed to sharply decrease in the PBMs and SBMs, reaching a minimal expression at the meristem tip (fig.33B-C). Expression was strong at the base of the spikelet but again was reduced in FM (fig.33E).

Therefore, *FT-L1* is not expressed in newly divided cells of primary and secondary meristems, but its

transcription increases and accumulates quickly at the base during meristem growth.

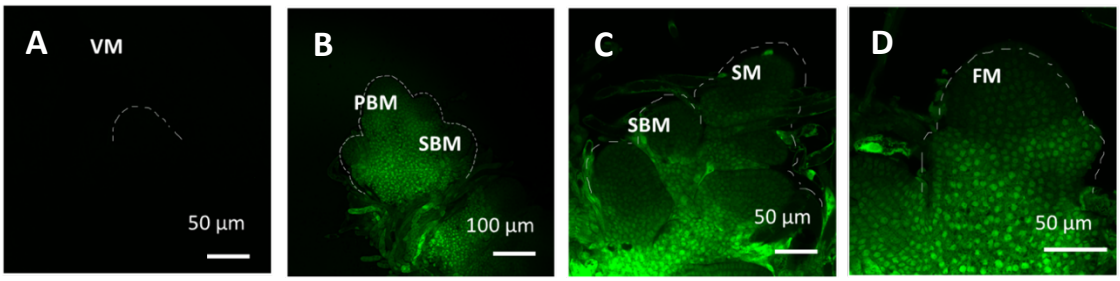

Figure 33- Spatial expression of FT-L1 based on pFT-L1:eYFP marker lines*. Longitudinal sections, 50 µm thick, of shoot apices positive to the transgene were imaged at the confocal Nikon Eclipse Ti2 inverted microscope. Meristems were sampled at vegetative meristem (VM; A), primary and secondary branch meristems (PBM and SBM; B), secondary branch and spikelet meristems (SBM and SM; C) and spikelet with floret meristems (SM with FM; D) stages. Green signal represents the fluorophore eYFP. Three independent pFT-L1:eYFP lines gave similar results. Experiments shown were repeated five times.*

4.1.4 FT-L1 operates in a cell-autonomous manner

For a deeper analysis of FT-L1 expression and to allow protein localization analysis we have generated *pFTL1:FTL1:eYFP* translational marker lines cloning the *FT-L1* coding sequence under control of the *FT-L1* promoter and in frame with the eYFP. We chose, among several T1 independent lines that were positive by PCR, those that were early flowering, suggesting that the fusion protein was functional. We used the WT as negative control.

To validate this signal pattern we used an independent approach through a collaboration with Daisuke Miki (Shanghai Center for Plant Stress Biology) who obtained *FT-L1:GFP* genomic lines (*gFT-L1:GFP*) by recombining the GFP directly into the rice genome, next to *gFT-L1* with the knock-in GFP approach. The researcher was working on gene targeting (GT) of Arabidopsis when we started collaborating and managed to adapt it to rice.

GT is the integration or replacement of a particular sequence, that can be achieved with combinations of engineered Sequence- Specific Nucleases (SSNs) and repair donor templates[96,97].

For this technique the *FT-L1–GFP* donor construct was transformed into a parental rice plant line, that already expressed Cas9 from a constitutive strong maize Ubiquitin 1 promoter. The *FT-L1–GFP* gene targeting construct harbors a Homology-Directed Repair (HDR) donor sequence with homology arms and an OsU6 promoter driven sgRNA cassette targeting the *FT-L1* locus.
By both approaches we obtained results with similar localization patterns, and, in fig.34A-F, a developmental time course merging the two different lines is presented.

During eYFP/GFP pattern analysis we note again the gradient from the base to the tip in both primary and secondary branch meristems and how it resembles the pattern of *Hd3a* protein localization in the *pHd3a:Hd3a–GFP* lines[48] (fig.35A-F).

We have therefore decided to comment our result in parallel, together with the discussion comparing the two proteins' patterns.

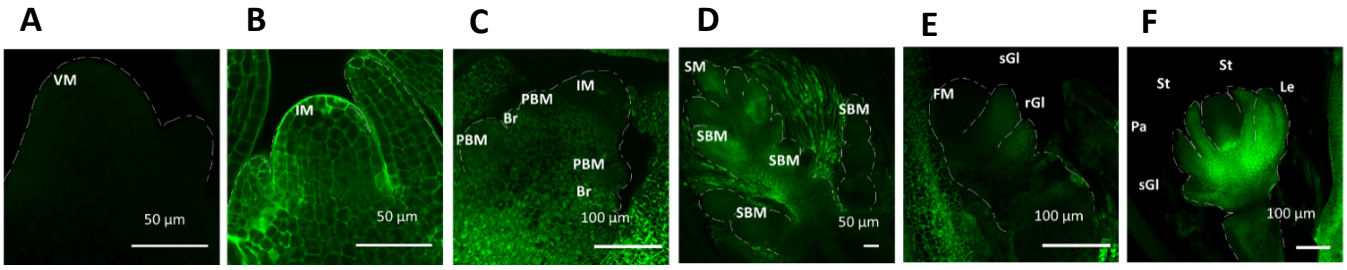

Figure 34- Spatio-temporal accumulation of the FT-L1 protein based on gFT-L1:GFP and pFT-L1:FT-L1:eYFP marker lines. *Longitudinal sections, 50 µm thick, of shoot apices positive to the transgene were imaged at the confocal Nikon Eclipse Ti2 inverted microscope and Zeiss LSM880 laser scanning confocal microscope. Stages included VM (**A**), IM (**B**), PBM (**C**), SBM and SM (**D**), SM and FM (**E**), FM (**F**). St, stamens; Pa, palea; Le, lemma; rGl, rudimentary glumes; sGl, sterile glumes. Green signal represents the fluorophore eYFP. Experiments shown were repeated five times and this panel includes pictures from both the knock-in and translational marker lines approaches.*

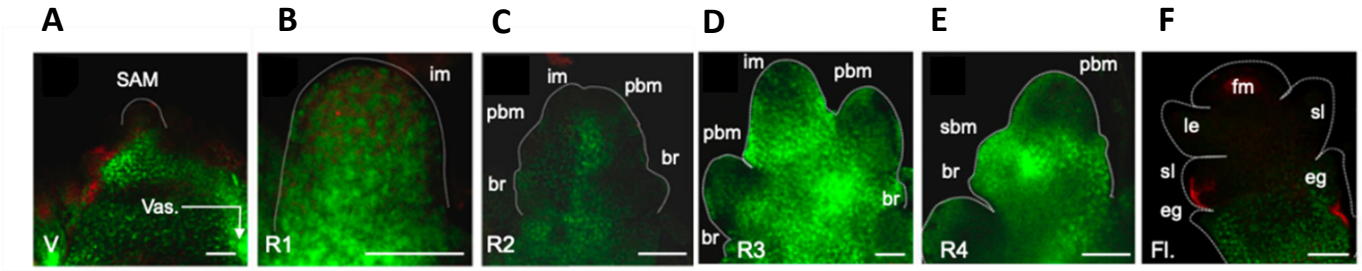

Figure 35 - Hd3a protein localization in in pHd3a:Hd3a-GFP transgenic plants at the shoot apex at different stages (R1–R4) of the inflorescence meristem and FM. *A. V, vegetative-stage plants. Vas, stem vasculature. B. R1, initial stage of floral transition with first bract formation. im, inflorescence meristem. C. R2, early stage of primary branch meristem initiation. br, bract; pbm, primary branch meristem. D. R3, late stage of primary panicle branch initiation. E. R4, final stage of primary branch formation and initiation of secondary branch meristem (sbm). F. Fl., floral organ development after R4. eg, empty glume; fm, floret meristem; le, lemma; sl, sterile lemma. (Scale bars, 50 µm.)* [48]

In the V meristems of these lines, similarly to *gFT-L1:GFP*, the GFP signal is missing (fig.34A and fig.35A). After the commitment, when the transition VM-to-IM (R1) occurs, both proteins were detected throughout the whole meristem. In particular, in FT-L1 lines a strong localization signal is also observed in the L1 layer (fig.34B and fig.35B). At the PBM stage (R2, R3), GFP signal was detected in the entire meristem, but was slightly weaker at the top of the inflorescence meristem and in newly developing primary branch meristems. As in FT-L1 lines the expression follows an expression gradient stronger at the PBM base and feeble at the tip of the same (fig.34B and fig.35C,D). At the PBM and SBM stages (R3,R4) Hd3a–GFP protein continued to accumulate in the primary branch meristems and the lower part of the shoot apex, as the signal became less detectable in the meristem. FT-L1–GFP signal is persisting, with protein localizing in particular in PBMs, SBMs and in the bracts, with a lower expression in the tip of these meristems and a decreased one in whole reproductive meristems themselves as for Hd3a-GFP lines (fig.34C,D and fig.35D,E).

In the Spikelet Meristem (fig.34E) FT-L1 accumulated in sterile and rudimentary glumes but lacked in the tip, where the Floret Meristem is forming.

In fig.34F, however, the FT-L1 signal is very strong in some floret structures such as stamen primordia, palea, lemma and glumes.

Differently, at this floret stage (FI), Hd3a-GFP fluorescence was detected only in the lower part of the meristem, in particular in the empty glumes, but is absent in the upper organs (fig.35F).
In the article, the authors suggested that Hd3a participates in inflorescence development due to the presence

of the GFP in SBM during the floral transition. Therefore, these data indicate that FT-L1 and Hd3a are often present in the same cells of the developing inflorescence.

For FT-L1 in general, transcriptional and translational patterns indicate decreasing expression at the tip of PBMs and SBMs. We interpret this expression pattern as required to avoid precocious meristems determination, and therefore a block in branching.
Finally, since overlapping patterns for transcriptional and translational markers were observed, even if we cannot exclude movement of the FT-L1 protein, we suggest that FT-L1 functions in a cell-autonomous manner at the meristem, during the commitment and subsequent stages of floral development.

4.2 MUTATIONS IN *FT-L1* DELAY FLOWERING TIME

Due to the high sequence similarity with Hd3a and RFT1, we hypothesized that FT-L1 could be redundant to the two florigens, suggesting a role for this gene in the control of flowering time.
Furthermore, the only publication in literature that mentions *FT-L1* suggests it has, indeed, a role in flower induction upon overexpression[18].

4.2.1 CRISPR ft-l1 mutants in Nipponbare

In order to confirm this hypothesis, CRISPR *ft-l1* mutant lines were generated in these three different backgrounds: Nipponbare Wild Type, Nipponbare *hd3a* and *rft1* single mutants. The *hd3a* and *rft1* single mutants are knock-out alleles: *hd3a-3*, with a T deletion in 86 position and *rft1-1*, with an A insertion in position 68, in the coding regions (*Mineri et al., manuscript submitted*).
The CRISPR mutants were generated to express a double sgRNA, which we selected to be in regions that were specific and with low chances of producing off targets, particularly in the closely related *Hd3a* and *RFT1* sequences (fig.36).

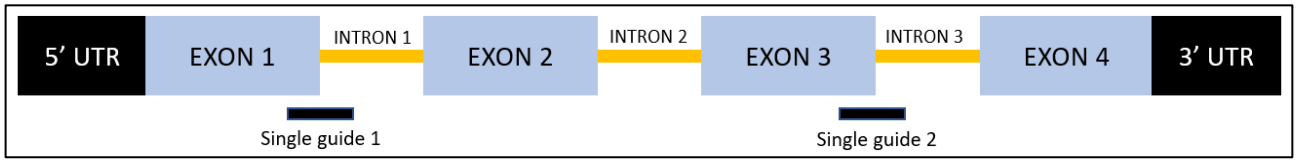

***Figure 36 - Scheme of the FT-L1 gene**. FT-L1 gene is organized in 4 exons and 3 introns. The two single guides designed for the editing experiment are represented with black lines. sgRNA 1 is designed between the first exon and the first intron, while sgRNA 2 is between the third exon and the third intron. Black boxes represent 5' and 3' UTRs; Blue boxes are the exons while yellow lines are the introns. Size of the aforementioned elements is not drawn to scale.*

For this, sgRNA OLIGO 1 is located between the first exon and the first intron, while sgRNA OLIGO 2 is between the third exon and the third intron. This strategy is aimed at splicing donor site disruptions, that would lead to intron retention or shifting splicing sites (fig.36,37).

The choice of using two guides was considered to increase the probability of cutting, because of the uncommonly designed position and because of the very low seed number for *hd3a* and *rft1* stable lines.

The rationale behind using *hd3a* and *rft1* as backgrounds was to test if there was any dose effect on the phenotype considered. The T0 population obtained presents mutations both in frame and out-of-frame (fig.37).

After having obtained and selected the alleles for both oligos, I've analyzed heading dates of the T1 plants both in SD and LD conditions (fig39A and fig.39B,C).

mutant	*ft-l1 -1*	*ft-l1 -2*	*ft-l1 -3*	*hd3a ft-l1 -4*	*hd3a ft-l1 -5*	*hd3a ft-l1 -6*	*hd3a ft-l1 -7*	*rft1 ft-l1 -8*	*rft1 ft-l1 -9*	*rft1 ft-l1 -10*	*rft1 ft-l1 -11*	*rft1 ft-l1 -12*	*rft1 ft-l1 -13*
OLIGO 1	C / E	I / I	WT / WT	C / X	C / O	C / C	A / Y	Q / Q	P / X	F / F	C / L	K / W	I / I
OLIGO 2	1 / 1	1 / 1	1 / 1	1 / 7	1 / 9	1 / 1	1 / 3	1 / 3	1 / 11	1 / 1	10 / 13	5 / 10	1 / 1

Figure 37 - Description of FT-L1 CRISPR mutant lines. *Table represents mutant alleles of FT-L1 in these genetic backgrounds: ft-l1 k.o. single mutants, hd3a ft-l1 k.o. double mutants and rft1 ft-l1 k.o. double mutants. The alleles generated by sgRNA 1 are indicated with letters, those generated by sgRNA 2 are indicated with numbers. The resulting genotypes can be complex, e.g. ft-l1-7 harbors alleles A and Y at the sgRNA1 position, and alleles 1 and 3 at the sgRNA2 position. See also Fig.38.*

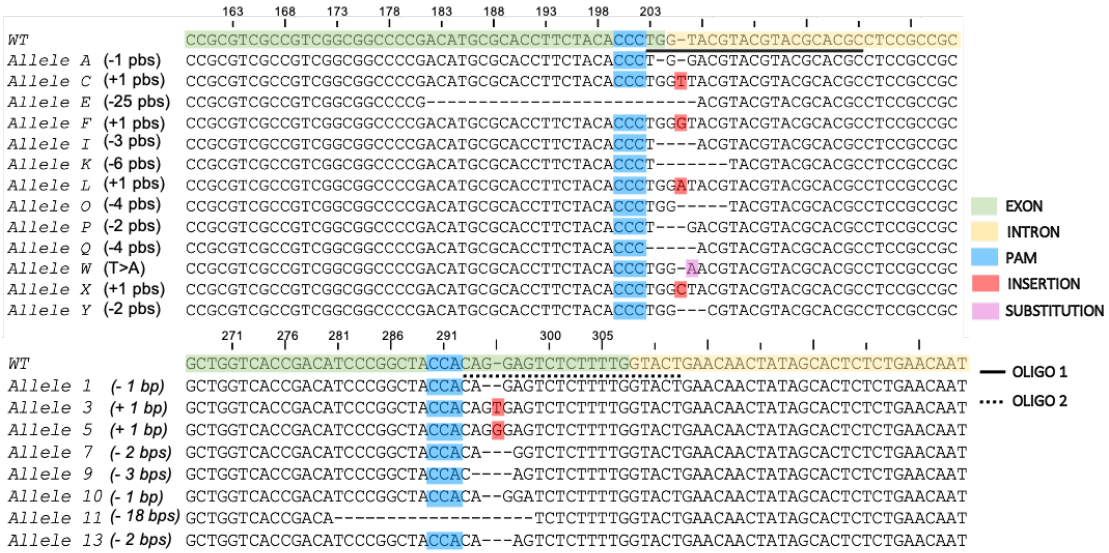

Figure 38 - Sequences of ft-l1 mutant alleles aligned against the wild type. *The alleles are the same shown in fig.37 and are aligned with MAFFT. As shown in the legend, the position of the sgRNAs is underlined in the WT allele. This figure is framed around the oligos location.*

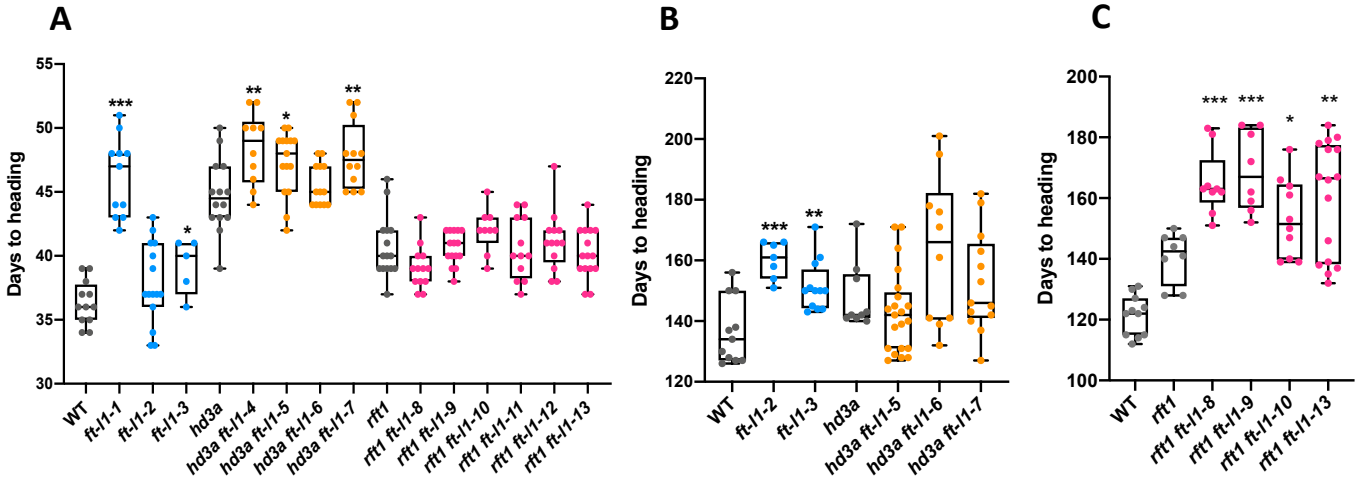

Figure 39 - Flowering time of ft-l1, hd3a ft-l1 and rft1 ft-l1 mutants. *A. Plants were grown for 2 months under LD conditions and then induced to flowering by shifting them to SDs. Days to heading were calculated starting on the day of the shift. B.,C. Plants were grown under LD. Days to heading were measured after sowing. Graphs in B and C are separated because referring to different experiments with independent WTs. Data are presented using box plots.. Each dot represents one plant and box plots in A.,B. and C. and are color-coded depending on the genotype, background controls are shown in grey. Each genotype is described in fig.37.*
** P<0.05, ** P<0.01 and *** P<0.001 based on unpaired two-tailed Student's t-test with Welch correction, measured relative to corresponding controls: ft-l1 vs. wild type, hd3a ft-l1 and rft1 ft-l1 vs. single hd3a and rft1 mutants, respectively.*

In the SD experiment (fig.39A), it is possible to observe a delay in flowering time for *ft-l1* mutant lines obtained in Nipponbare wild type background. In particular, this delay was in the lines *ft-l1-1* and *ft-l1-3* which flower on average 39.2 and 46 days after the shift into inductive conditions for flowering.

On the other hand, *ft-l1-2* does not display a delay in heading date, on average 37.8 DAS, respect to the control, which flowers on average after 36 days. These data indicate that *FT-L1* promotes the transition from VM to IM.
Moreover, an additive delay in heading date has been observed for double *hd3a ft-l1* mutant plants compared to the single mutants. Thus, under SD, *FT-L1* and *Hd3a* have additive effects on promoting flowering.
For what concerns *rft1 ft-l1*, instead, we observed the same phenotype of *rft1* single mutants with any additional delays.
We have performed the same analysis also in LD conditions (fig.39B,C) on a reduced number of lines because, in LD, heading date analysis on florigens mutants takes longer to be completed and plants are more prone to get sick due to fungal infections.

In this analysis, *ft-l1* mutants displayed delay in the heading for *ft-l1-2* and *ft-l1-3* genotypes, considered while in double *hd3a ft-l1* lines no delay was detected when compared to the single *hd3a.*
For double *rft1 ft-l1* lines we performed the experiment more than once, because of multiple fungal infections, maybe caused by an oversensitivity to rice blast or simply due to longer time spent by plants in the growth chamber. We observed a very strong delay in all *rft1 ft-l1* lines in respect to the *rft1* single. In these conditions, the addictive effect was observed between *FT-L1* and *RFT1* but not between *FT-L1* and *Hd3a*.

These data suggest that *FT-L1* enhances the flowering inducing effects of *Hd3a* or *RFT1* depending on the photoperiodic conditions.

As described previously[8,17,98], the rice florigens are not expressed equally in both photoperiods: in SD conditions both *Hd3a* and *RFT1* are expressed, while in LD conditions only *RFT1* is expressed. Due to different expression and regulation of Hd3a and RFT1, *ft-l1* could play an additional role on flower induction in a different manner.
In LD conditions and in absence of *RFT1* (and *FT-L1*), indeed, *Hd3a* expression is anyway residually activated after a long time - validating the redundancy of two florigens - causing a very strong delayed flowering phenotype. In SD conditions the rationale is the same but the effect is milder since *RFT1* has still am expression in inductive conditions.

Therefore, we can conclude that FT-L1 acts downstream of both florigens at the meristem during the transition from vegetative to inflorescence stage, proposing a model where FT-L1 is part of a feed-forward regulatory loop necessary for a fine-tuned commitment.

4.2.2 EMS FT-L1 mutants in Volano

Taking into consideration these phenotypes, and in order to exploit *FT-L1* mutations, we wanted to further test phenotypes in a different genetic background and under natural photoperiods.
For this purpose, we took advantage of sodium azide mutants isolated from a Volano collection. Volano is an Italian variety adapted to Northern latitudes, insensitive to photoperiod due to a natural background mutation in *Hd1*[9]. Therefore, it flowers relatively early also in natural long photoperiods, typical of the Italian cropping season.

We screened 4000 M2 individuals of the Volano collection, exploiting the KeyPoint™ technology by KeyGene. This high-throughput technique, based on a multi-dimensional pool scheme, allows to identity mutations in a sequence of interest by amplifying each template with tags specific for each multi-dimensional pool. After gene-specific amplification, next-generation sequencing was performed to assign genotypes to each individual plant[99].

We isolated three different *FT-L1* alleles, producing the protein variants FT-L1^{P95S}, FT-L1^{T145I} and FT-L1^{G117R} whose aminoacidic substitutions are in highly-conserved residues of the protein (fig.40A,B).

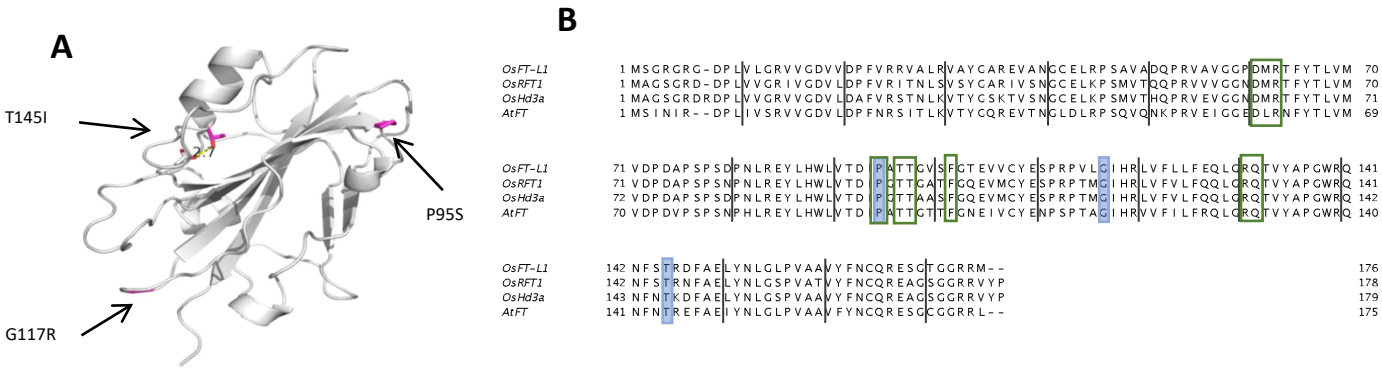

Figure 40 - Presentation of FT-L1 EMS mutants. *A. 3D structure of FT-L1, highlighting the amino acidic substitutions isolated from a mutagenized collection in Volano. Modified residues are highlighted in pink. B. Alignment of FT-L1 with RFT1, Hd3a and Arabidopsis thaliana FT. Green boxes highlight the conserved amino acidic residues involved in binding with Gf14 proteins. The three conserved amino acids in blue boxes are those mutated in the FT-L1 Volano lines.*

These three mutations, according to DUET (http://bleoberis.bioc.cam.ac.uk/duet/), could be divided in two different groups depending on the localization and the predicted effect of the mutation on protein stability. For P95S and G117R, the mutations localize on the surface and modify charge, having a predicted destabilizing effect, whereas for T145I, the mutation is in the core and no destabilization is predicted (fig.41).

FT-L1 WT	FT-L1 mutants	DUET Predicted Stability Change (ΔΔG)	Surface/core
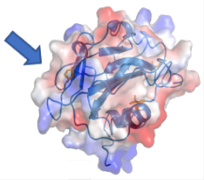	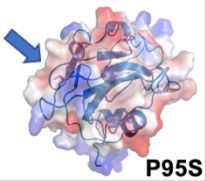 P95S	-1.487 Kcal/mol (Destabilizing)	SURFACE
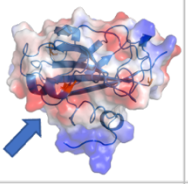	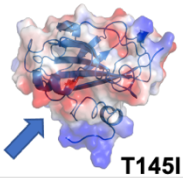 T145I	0.944 Kcal/mol (Stabilizing)	CORE
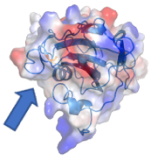	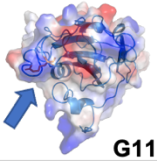 G117R	-1.217 Kcal/mol (Destabilizing)	SURFACE

Figure 41 - 3D visualization of Volano FT-L1 mutants using Pymol. *The surface electrostatic potential is shown on the tertiary structure. Blue indicates a positively charged surface, red a negatively charged surface. In the same table, the localization of mutated residues is indicated, along with protein stability changes computed using DUET.*

The P95S substitution is likely to be the strongest since it falls in an amino acidic residue already published to be required for Hd3a–14-3-3 protein-protein interaction (the residue is P96 in Hd3a and the 14-3-3 protein is the Gf14c)[60].

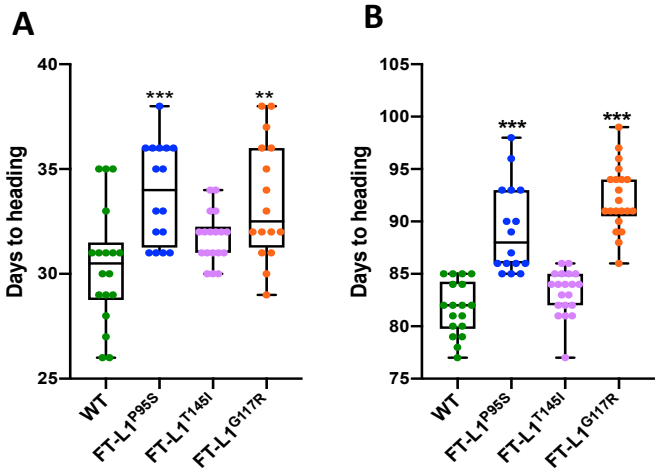

Figure 42 - Flowering time of FT-L1 Volano mutants under SD (A) and natural LD in the field (B).
*Flowering time under SD conditions has been run in greenhouses while flowering time under NATURAL LD has been performed in a Vercelli field. Each dot represents one plant and is color-coded depending on the genotype. ** P<0.01 and *** P<0.001, p values are obtained by unpaired two-tailed Student's t-test with Welch correction, measured relative to the WT. Days to heading for SD (A) are days from the shift LD-> SD while for N-LD (B) are days from the sown.*

We therefore decided to carry out analyses on flowering time of these Volano mutations, using different growth conditions as SD and natural LD field condition in Vercelli, Italy (fig.42A,B).

What emerged was that the mutants display a different flowering phenotype depending on the mutation. The *FT-L1*^{P95S} and *FT-L1*^{G117R} mutants display a strong phenotype of delay both in SD and LD conditions, while *FT-L1*^{T145I} does not show any statistically significant delays in flowering compared to WT on both grown conditions tested.

Consistently, the days to flower in SD and LD conditions for the WT are not so much different, this is caused by Volano reduced sensitivity to the photoperiod, as mentioned before.
This phenotype of delayed flowering is validating the heading date data observed in CRISPR mutant lines. Taken these evidences, we can assume *FT-L1* promotes flowering after the commitment, both under LD an SD conditions, in a synergistic and addictive manner with *Hd3a* and *RFT1*.

4.3 MUTATIONS IN *FT-L1* AFFECT PANICLE ARCHITECTURE AND FERTILITY

By observing the panicles of Volano growing in the field, we noticed they looked denser, differently from WT ones (fig.45A-D). We then decided to analyze all panicle traits with the P-TRAP software[100], including branch numbers and rachis length, in order to identify and quantify the traits responsible for the altered phenotype and, eventually, whether there would be any direct consequences on yield.
In SD conditions (fig.43A), *FT-L1*^{P95S} and *FT-L1*^{G117R} plants showed a statistically significant increase in the number of secondary branches, while *FT-L1*^{T145I} did not, compared to wild type plants.
In LD conditions (fig.43B), all mutants increased the number of branches. *FT-L1*^{P95S} and *FT-L1*^{G117R} produced even tertiary branches, while *FT-L1*^{T145I} increased only the number of secondary ones.
Differently, for what concerns the number of primary branches no change was detected in any conditions and in any lines tested.

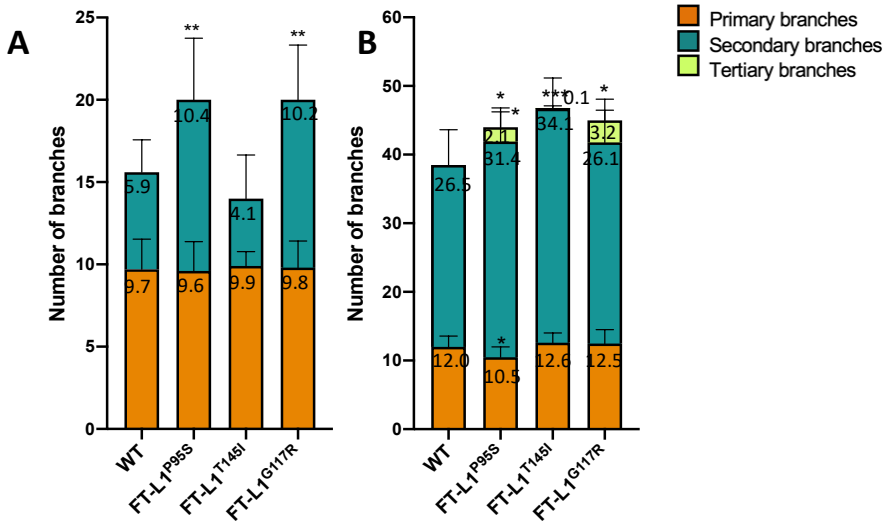

Figure 43 - Quantification of panicle branching in FT-L1 Volano mutants under SD (A) and natural LD in the field (B). *Data were obtained with the P-TRAP software[100] and indicate the mean ± standard deviation of ten panicles per genotype collected from the main culms (means are reported on the histograms). * P<0.05, ** P<0.01 and *** P<0.001 are based on unpaired two-tailed Student's t-test with Welch correction.*

Interestingly, *FT-L1*^{T145I} in SD shows no changes neither in the heading date nor in the panicle architecture, while in LD it produced more secondary branches but no delay in flowering time was recorded. These evidences indicate that the effects of FT-L1 on flowering and panicle architecture are genetically separable and that an increase in the number of branches is not just a consequence of a delay of flowering.

As mentioned above[6], the panicle is shaped by new meristems that are generated sequentially by axillary meristems, gaining their identity in a time- and position- dependent manner. This increase in the number of secondary branches points out that FT-L1 has a role in promoting spikelet meristem identity. With a reduced activity of FT-L1, transition from SBMs to SM is delayed causing a decrease in panicle determinacy and thus a reversion of SM to SBM fate.

To further assess if these architectures are due to changes in FT-L1/florigens abundance during panicle development, we have checked panicles of *FT-L1* and *Hd3a* over-expressor lines (fig.44A).

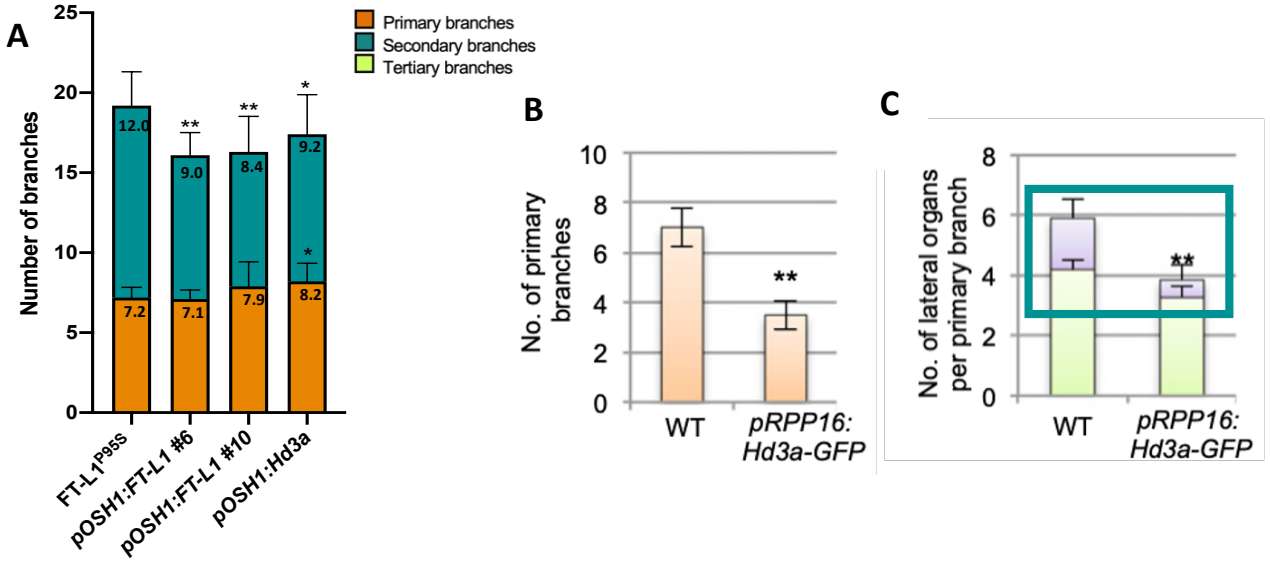

Figure 44 – Quantification of panicle traits in over-expressor lines. *A. Quantification of panicle branches in over-expressor lines under LD. Data were obtained with the P-TRAP software[100] and indicate the mean ± standard deviation of ten panicles per genotype collected from the main culms (means are reported on the histograms). * P<0.05 and ** P<0.01 are based on unpaired Student's t-test with Welch correction. B.-C. Inflorescence phenotype of Hd3a-overexpressing plants[48]. B. number of primary branches per panicle C. number of lateral organs per primary branch. Light green and purple bars indicate number of flowers and number of secondary branches respectively. Green-boxed are pointed out the secondary branches[48].*

For what concerns the *pOSH1:FT-L1* lines, we quantified a decrease in the number of secondary branches compared to the background control, consistent with previous data collected for the mutants and with the hypothesis of FT-L1 promoting SM formation and determinacy.
Not only *pOSH1:FT-L1* but also *pOSH1:Hd3a* line showed a lower number of secondary branches, corroborating what was previously observed by Tamaki et al. in pRPP16:Hd3a–GFP plants with reduced numbers of primary branches and of secondary branches[48] (fig.44B,C).

These results suggest that, together with FT-L1, Hd3a may have an additional function, along with VM-to-IM conversion, in promoting the inflorescence-to-flower transition in the reproductive meristem.

In fig.45A-E it is possible to notice the panicles' picture of Volano FT-L1 EMS mutants and over-expressors.

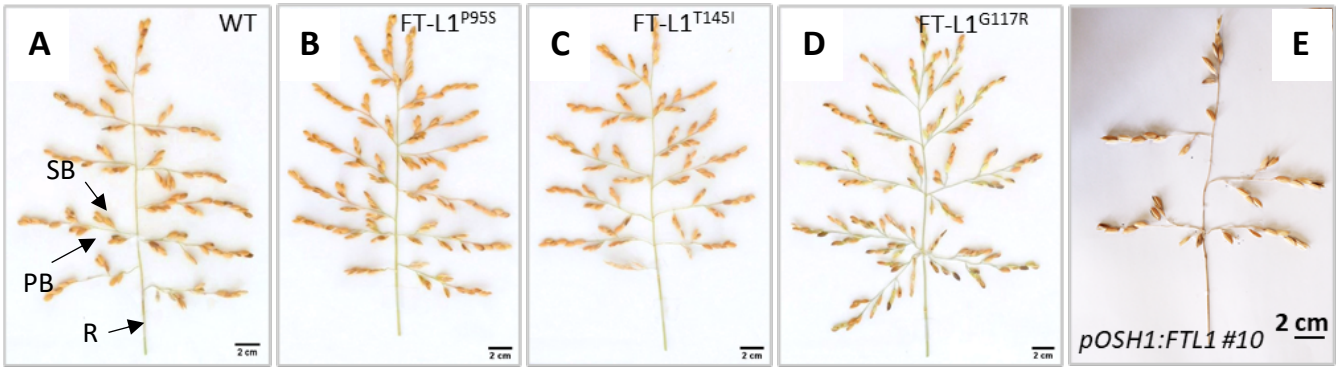

Figure 45 - Representative pictures of Volano panicles of the indicated genotypes. *A. Volano WT; B. Volano FT-L1^{P95S}; C. Volano FT-L1^{T145I}; D. Volano FT-L1^{G117R}; E, Volano pOSH1:FT-L1 #10. R, Rachis; PB, Primary Branch, SB, Secondary Branch. Scale bar, 2 cm.*

We next wanted to investigate if an increase in secondary branch number correlates with an increase in the yield of Volano mutants. To this end, we have performed also an analysis of the grains, comparing the results with the wild-type control, quantifying caryopsis numbers (fig.46).

For this analysis we have taken into consideration the total number of flowers and the number of aborted/sterile flowers per panicle of the same plants used for the branches analysis.

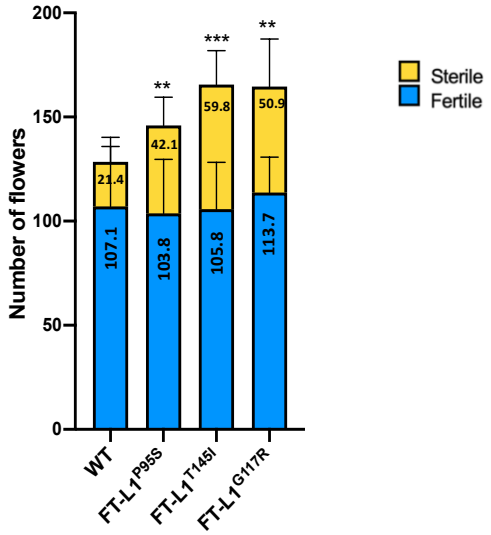

Figure 46 - Quantification of panicle fertility in FT-L1 Volano mutants*. Data indicate the mean ± standard deviation of flowers, fertile and sterile, collected from the ten panicles analyzed with the P-TRAP software. The means are reported on the histograms. ** P<0.01 and *** P<0.001 are based on unpaired two-tailed Student's t-test with Welch correction. Sterile flowers are those not giving rise to a caryopsis or those aborting it precociously.*